

Activation of the STING-Dependent Type I Interferon Response Reduces Microglial Reactivity and Neuroinflammation

Highlights

- Ganciclovir induces type I interferon signaling and modulates microglial reactivity
- Microglial reactivity is associated with upregulation of innate immune adaptor STING
- Ganciclovir inhibits microglial inflammation in EAE mouse model through STING

Authors

Vidhu Mathur, Ritwik Burai, Ryan T. Vest, ..., Lingyin Li, Hilal A. Lashuel, Tony Wyss-Coray

Correspondence

twc@stanford.edu

In Brief

Mathur et al. describe a non-canonical function of the antiviral drug ganciclovir in microglia. Ganciclovir induces a type I interferon response and reduces neuroinflammation in a mouse model of multiple sclerosis. The innate immune adaptor STING is required for this activity of ganciclovir.



Activation of the STING-Dependent Type I Interferon Response Reduces Microglial Reactivity and Neuroinflammation

Vidhu Mathur,^{1,4} Ritwik Burai,⁵ Ryan T. Vest,² Liana N. Bonanno,¹ Benoit Lehallier,¹ Macy E. Zardeneta,⁴ Karishma N. Mistry,⁴ Danny Do,¹ Samuel E. Marsh,⁶ Edsel M. Abud,⁶ Mathew Blurton-Jones,⁶ Lingyin Li,³ Hilal A. Lashuel,⁵ and Tony Wyss-Coray^{1,4,7,*}

¹Department of Neurology and Neurological Sciences, School of Medicine

²Chemical Engineering Graduate Program, School of Engineering

³Biochemistry Department, School of Medicine
Stanford University, Stanford, CA 94305, USA

⁴Center for Tissue Regeneration, Repair and Rehabilitation, VA Palo Alto Health Care System, Palo Alto, CA 94304, USA

⁵Laboratory of Molecular and Chemical Biology of Neurodegeneration, Brain Mind Institute, Station 19, School of Life Sciences, Ecole Polytechnique Fédérale de Lausanne (EPFL), CH-1015 Lausanne, Switzerland

⁶Institute for Memory Impairments and Neurological Disorders, University of California, Irvine, Irvine, CA 92697, USA

⁷Lead Contact

*Correspondence: twc@stanford.edu

<https://doi.org/10.1016/j.neuron.2017.11.032>

SUMMARY

Brain aging and neurodegeneration are associated with prominent microglial reactivity and activation of innate immune response pathways, commonly referred to as neuroinflammation. One such pathway, the type I interferon response, recognizes viral or mitochondrial DNA in the cytoplasm via activation of the recently discovered cyclic dinucleotide synthetase cGAS and the cyclic dinucleotide receptor STING. Here we show that the FDA-approved antiviral drug ganciclovir (GCV) induces a type I interferon response independent of its canonical thymidine kinase target. Inhibition of components of the STING pathway, including STING, IRF3, Tbk1, extracellular IFN β , and the Jak-Stat pathway resulted in reduced activity of GCV and its derivatives. Importantly, functional STING was necessary for GCV to inhibit inflammation in cultured myeloid cells and in a mouse model of multiple sclerosis. Collectively, our findings uncover an unexpected new activity of GCV and identify the STING pathway as a regulator of microglial reactivity and neuroinflammation.

INTRODUCTION

Neurodegenerative diseases such as Alzheimer's disease, Parkinson's disease, Huntington's disease, multiple sclerosis, fronto-temporal dementia, and amyotrophic lateral sclerosis are associated with activation of predominantly innate immune pathways, referred to as neuroinflammation. During this process, microglia and other brain cells and, in some cases, infiltrating cells from the systemic environment secrete

inflammatory cytokines and chemokines with positive and negative effects on the brain (Glass et al., 2010). Interferons are one such class of cytokines with neuroprotective and neurotoxic properties (Deczkowska et al., 2016). For example, the type II interferon, IFN γ , previously considered proinflammatory, has recently been shown to contribute to immune surveillance in healthy brains (Kunis et al., 2013). Similarly, the type I interferon IFN β was shown to negatively affect brain function during aging (Baruch et al., 2014), and on the other hand, IFN β can serve a protective function and is used to dampen inflammation in active, relapsing multiple sclerosis (Group, 1993). Additionally, the lack of IFN β signaling in neurons resulted in Lewy body and Parkinson's disease-like dementia in mice (Ejlerskov et al., 2015). Together, these studies suggest that the relative levels of type I and type II interferons and the context in which they act have a profound effect on neuroinflammation and neurodegeneration (Deczkowska et al., 2016).

The production of type I interferons can be induced by a number of pattern recognition receptors (Takeuchi and Akira, 2010), which trigger signaling cascades and targeted immune responses. The presence of double-stranded (ds) viral DNA in the host cytoplasm, for example, is recognized by the recently discovered cyclic GMP-AMP synthetase (cGAS), which catalyzes production of the second messenger 2'3'-cyclic-GMP-AMP (cGAMP), a potent ligand of the signaling adaptor known as stimulator of interferon genes (STING/MPYS/MITA/ERIS, encoded by *TMEM173*). This cascade further elicits activation of IKK and TBK1 kinases, NF- κ B, and IRF3 transcription factors and production of IFN β (Ishikawa and Barber, 2008; Okabe et al., 2009; Schoggins et al., 2011; Sun et al., 2009). STING has thus emerged as an attractive target for drug discovery, especially for cancer treatment (Ahn et al., 2015; Fu et al., 2015), but little is known about the role of STING in the brain and whether it has a role in neuroinflammation and neurodegeneration.



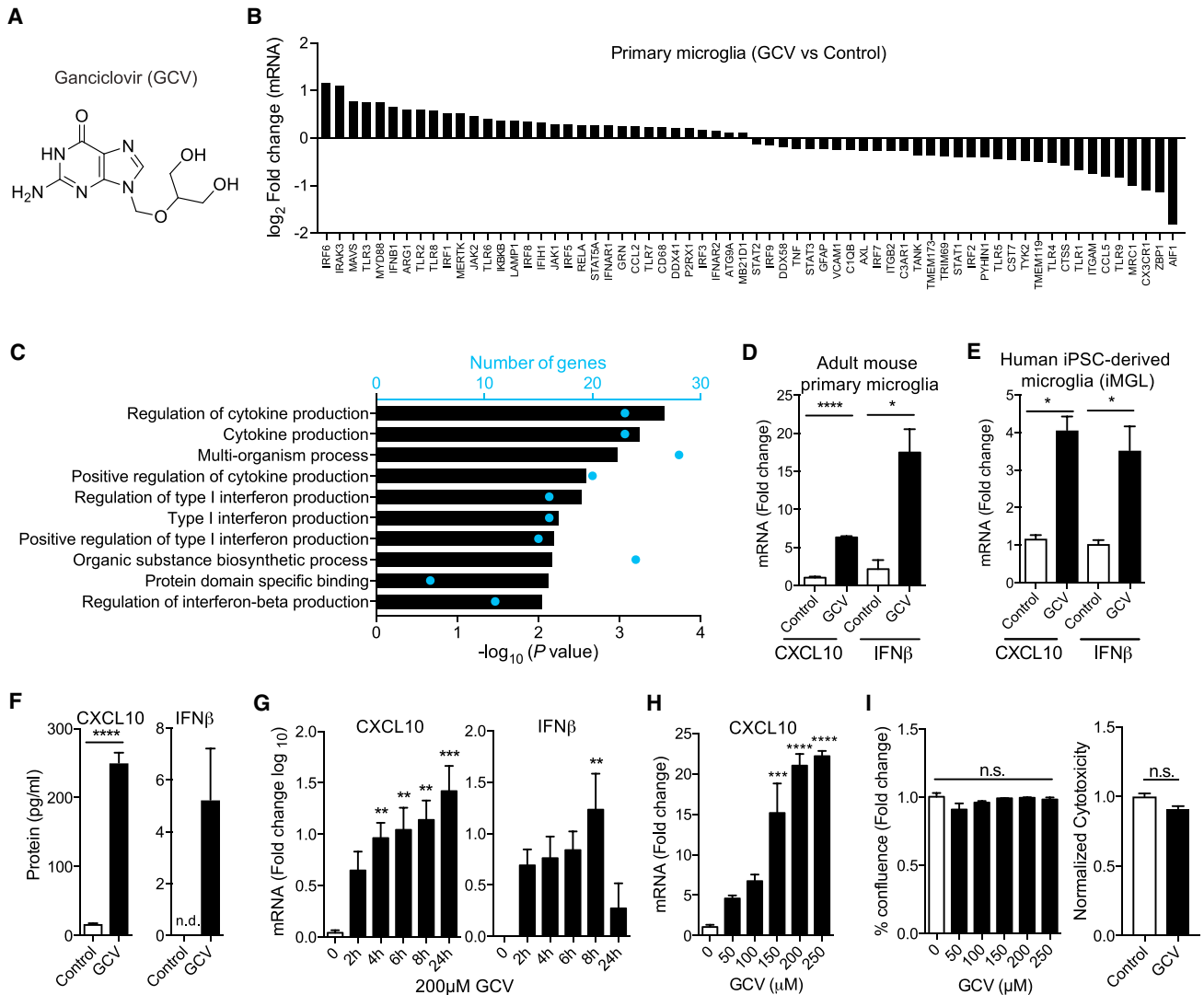


Figure 1. Ganciclovir Induces an Interferon Response in Microglia

(A) Structure of GCV.
 (B) Microfluidic qRT-PCR analysis of control or GCV-treated primary microglia from adult mice ($n = 4$ mice/group). Differentially expressed genes with \log_2 fold change > 0.1 and < -0.1 are shown.
 (C) Gene ontology pathways enriched by GCV treatment in primary microglia. Blue dots indicate the number of significant genes in the respective gene ontology (GO) term.
 (D and E) qRT-PCR analysis for CXCL10 and IFN β from GCV-treated primary microglia from adult mice (D) and iPSC-derived human microglia (iMGL) (E) for 24 hr.
 (F) ELISA for CXCL10 and IFN β on supernatants from primary microglia treated with GCV for 24 hr.
 (G) Time course for the induction of CXCL10 and IFN β mRNA in BV-2 cells treated with GCV for 24 hr.
 (H and I) Dose response for CXCL10 mRNA (H), cell viability (I, left), and cytotoxicity (I, right) in BV-2 cells treated with GCV for 24 hr.
 Fold change is based on control treatment for the experiment. All GCV treatments were performed with 200 μ M unless otherwise noted. Statistical tests: one-way ANOVA followed by Dunnett's multiple comparison test (G–I) and unpaired Student's t test (D–F). Error bars represent mean + SEM from 3 (cell lines) or 2 (primary cells) independent experiments. * $p < 0.05$, ** $p < 0.01$, *** $p < 0.001$, **** $p < 0.0001$.

Here, we show that the antiviral drug ganciclovir (GCV) induces a type I interferon response in microglia that depends on a functional STING pathway. *In vivo*, STING is expressed in microglia in the CNS and is upregulated in experimental autoimmune encephalomyelitis (EAE), a mouse model for multiple sclerosis. Treatment with GCV reduces STING expression, the microglial inflammatory signature, immune cell infiltration,

and paralysis in the EAE mouse model in a STING-dependent fashion.

RESULTS

GCV (Figure 1A) and other nucleoside analogs of 2'-deoxyguanosine are effective anti-viral drugs for the treatment of

cytomegalovirus and herpesvirus infections (Faulds and Heel, 1990). We recently reported that GCV, at therapeutic doses equivalent to those in humans, ameliorates the disease course and pathology of EAE in mice (Ding et al., 2014). GCV exerted these effects, in part, by reducing immune cell infiltration and inhibiting the proliferation of microglia, the immune cells of the CNS. To understand the molecular basis of GCV activity, microglia-like BV-2 cells were stimulated with GCV, and 38 secreted proteins were measured using a Luminex-based array (Figures S1A and S1B). GCV treatment led to the upregulation of several antiviral proteins, and CXCL10 was most significantly overproduced (Figure S1B). Gene expression analysis of GCV-treated BV-2 cells (Figures S1C and S1D) using a microfluidic qRT-PCR panel that we created (consisting of 86 microglia genes; Table S1) showed upregulation of CXCL10 and type I interferons (Figures S1C and S1D). To corroborate these findings, primary microglia isolated from adult mice were treated with GCV and analyzed using the microfluidic panel. As with BV-2 cells, primary microglia showed prominent induction of type I interferon-dependent gene expression after GCV treatment (Figures 1B and 1C), including CXCL10 and IFN β (Figure 1D). In addition, these genes were increased at the protein level as well (Figure 1F). Importantly, GCV not only activated this interferon response in mouse microglia but also in human induced pluripotent stem cell (iPSC)-derived microglia (iMGLs) (Abud et al., 2017; Figure 1E). We chose to use CXCL10 and IFN β as outcomes for GCV activity because these proteins were upregulated at transcript as well as protein levels across multiple microglial and myeloid cell types. GCV exhibited time- and dose-dependent activity without detectable toxicity (Figures 1G–1I). Hence, we conclude that these immune-modulatory effects of GCV are unlikely to be due to growth inhibition or cell death.

In its canonical mechanism of action, GCV is phosphorylated by viral thymidine kinases (e.g., herpes simplex virus type 1 thymidine kinase, HSVtk) (Littler et al., 1992) and incorporated into cellular DNA, inhibiting replication (Matthews and Boehme, 1988). In contrast, the GCV activity we describe did not require HSVtk or endogenous tk. The cells used in this study did not express viral tk (Figures S1E and S1F). Additionally, microglia isolated from adult tk1 knockout mice treated with GCV also produced CXCL10 and IFN β (Figures S1G and S1H), suggesting that thymidine kinase is dispensable for this activity of GCV.

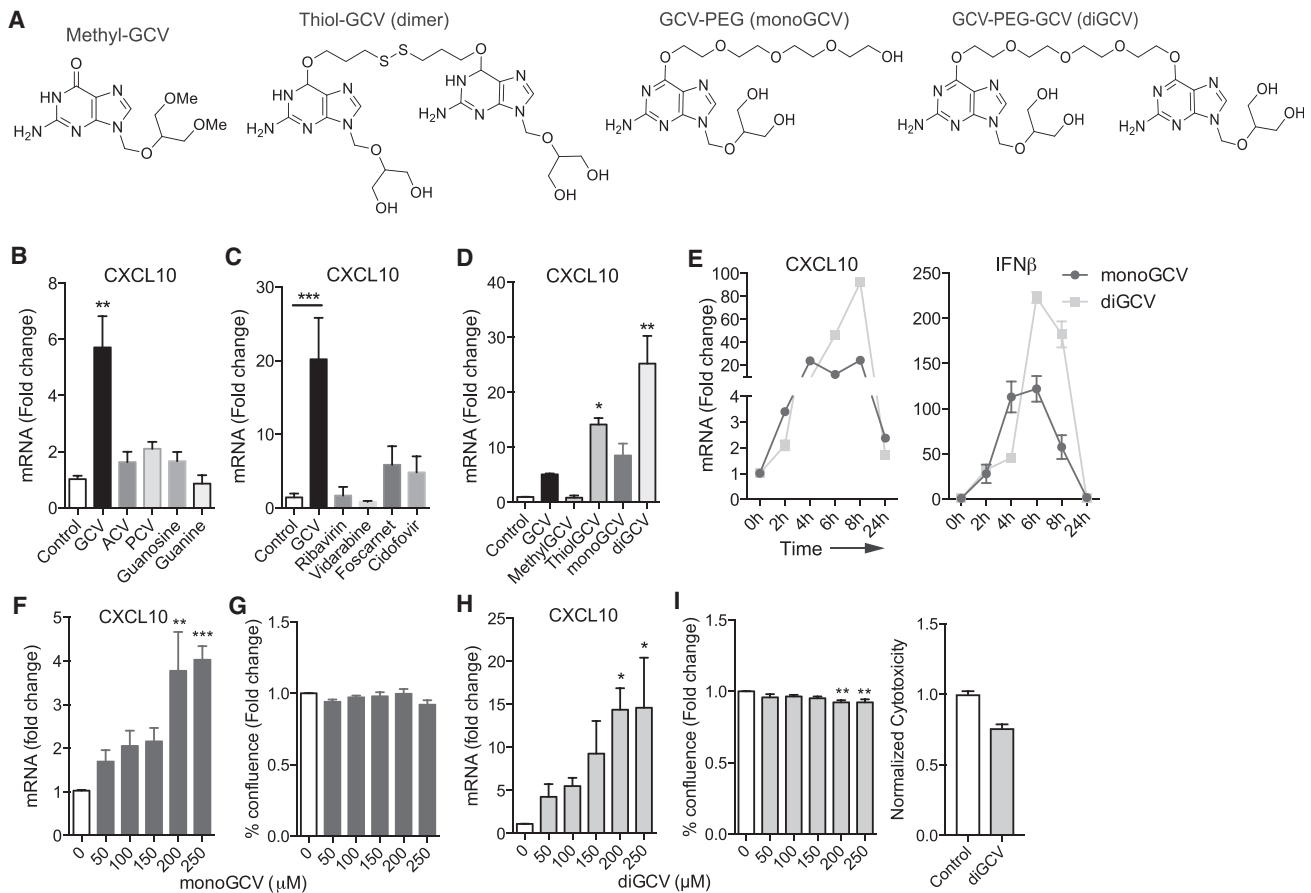
In a cell-based model of inflammation where primary microglia or BV-2 cells were stimulated with IFN γ and lipopolysaccharide (LPS), GCV led to significant transcriptional inhibition of several proinflammatory genes (Figure S2A). One of the most significantly reduced transcript and protein was NOS2/iNOS (Figures S2A and S2C–S2E), which further led to a reduction in neurotoxic microglial nitric oxide production (Figures S2B and S2F).

We tested if other compounds and antiviral drugs could induce a type I interferon response like GCV. The structurally related FDA-approved GCV analogs acyclovir (ACV) and penciclovir (PCV), or the endogenous molecules guanine and guano-

sine and structurally unrelated anti-viral drugs (structures shown in Figure S3) failed to induce CXCL10 mRNA (Figures 2B and 2C), suggesting that the 1,3-dihydroxy-2-propoxymethyl group at N9 of the guanine ring is necessary for activity. In support of this notion, methylating the 1,3-dihydroxyl groups in GCV (MethylGCV) abrogated CXCL10-inducing activity, whereas providing 4 hydroxyl groups in GCV dimers synthesized using a reducible disulfide linker (thiol-GCV) or non-reducible polyethylene glycol (PEG) linkers (diGCV) at C6 of the guanine ring (structures shown in Figure 2A) increased potency to induce CXCL10 (Figures 2D and 2E). Like GCV, diGCV as well as the PEGylated GCV monomer (monoGCV) dose-dependently induced CXCL10 without causing considerable toxicity (Figures 2F–2I). Additionally, monoGCV and diGCV potently reduced iNOS transcript and protein (Figures S2C, S2D, and S2G) and nitric oxide production in IFN γ /LPS-stimulated BV-2 cells (Figure S2H), and they induced CXCL10 independent of endogenous tk1 (Figure S2I).

Interferons activate the Jak/Stat signaling pathway to induce CXCL10 (Liu et al., 2011), and we observed that GCV and diGCV similarly depend on this pathway (Figure 3). Specifically, the Stat1 inhibitor fludarabine (Frank et al., 1999) or the Jak kinase inhibitors ruxolitinib and TG101348 (Zhou et al., 2014) strongly inhibited CXCL10 production in response to GCV and diGCV (Figures 3A and 3F) without causing toxicity (Figures 3B and 3G). Likewise, small interfering RNA (siRNA) knockdown of Stat1 and Jak1, but not TLR3, reduced GCV activity (Figures 3C, 3H, and 3I). Primary microglia from Stat1 knockout (KO) mice also significantly reduced CXCL10 or IFN β mRNA induction by GCV, monoGCV, and diGCV (Figure 3D). Additionally, the ability of GCV to suppress the inflammatory marker iNOS was dependent on Stat1 (Figure 3E). GCV and its derivatives might activate the Jak/Stat pathway either directly or through the production and autocrine signaling of IFN β through subsequent feedback loops, activating other pattern recognition receptors (Figure 4A). Indeed, neutralization of IFN β with an antibody partly reduced CXCL10 induction mRNA by GCV, monoGCV, or diGCV in BV-2 cells (Figure 3J).

Recent studies have shown that, upon sensing exogenous dsDNA in the cytoplasm, the enzyme cGAS catalyzes the formation of cGAMP (structure in Figure S3), which subsequently induces a potent interferon response (Hornung et al., 2014; Ishikawa et al., 2009). Cyclic dinucleoside monophosphates (e.g., c-di-GMP; structure in Figure S3) can induce a similar response (Chin et al., 2013). These dinucleotides activate the endoplasmic reticulum (ER) membrane adaptor protein STING, which then activates TANK binding kinase 1 (Tbk1), NF- κ B, and IRF3 (Barber, 2015; Ishikawa and Barber, 2008) and downstream effector genes, including IFN β and CXCL10 (Figure 4A). Accordingly, and in line with previous studies (Gao et al., 2013), cGAMP and c-diGMP strongly induced CXCL10 and IFN β in microglia (Figure 4B), as did the reported STING agonists 5,6-Dimethylxanthone-4-acetic acid (DMXAA) and 10-carboxymethyl-9-acridanone (CMA) (Cavlar et al., 2013; Gao et al., 2013; Prantner et al., 2012; Figure 4C). GCV and diGCV also induced CXCL10 in the human monocyte cell line THP-1, whereas DMXAA, which is specific for mouse STING (Conlon et al., 2013), did not (Figure 4D). Due to its



apparent structural similarity, we hypothesized that diGCV, and possibly GCV cellular metabolites, may mimic cyclic dinucleotides and activate the STING pathway.

Excitingly, siRNA-mediated knockdown of STING in BV-2 cells largely abrogated the capacity of diGCV and, to a lesser extent, monomeric GCV to induce CXCL10 (Figure 4E). Moreover, primary microglia from STING^{gt/gt} mice, which lack functional STING protein (Sauer et al., 2011) and do not respond to cGAMP, failed to induce CXCL10 and IFN β mRNA in response to GCV, monoGCV, and diGCV (Figure 4F). Consistent with GCV targeting the STING pathway, pharmacological inhibition of Tbk1 activity using the antagonist amlexanox and siRNA-mediated knockdown of IRF3 inhibited the capacity of monomeric and dimeric GCV to induce CXCL10 mRNA (Figures 4G and 4H). Furthermore, siRNA-mediated knockdown of the upstream activator cGAS did not affect the activ-

ity of GCV and diGCV to induce CXCL10 (Figure 4I). These data in aggregate show that, like the reported STING agonists (Burdette et al., 2011; Cavlar et al., 2013; Gao et al., 2013), the ability of GCV and its derivatives to induce a type I interferon response in microglia-like cells requires a functional STING pathway and downstream Jak/Stat signaling. Native GCV and diGCV molecules did not bind strongly to purified mouse STING protein (Figure 4J). The possibilities that these molecules are prodrugs, which are modified intracellularly to be active, or that they bind to another target in the STING pathway remain to be elucidated.

To determine the involvement of STING in regulating microglial reactivity and neuroinflammation *in vivo*, we induced the autoimmune disease EAE in wild-type (WT) and STING^{gt/gt} mice and treated them with GCV (Figure 5A). We found that STING was specifically expressed in microglia and not

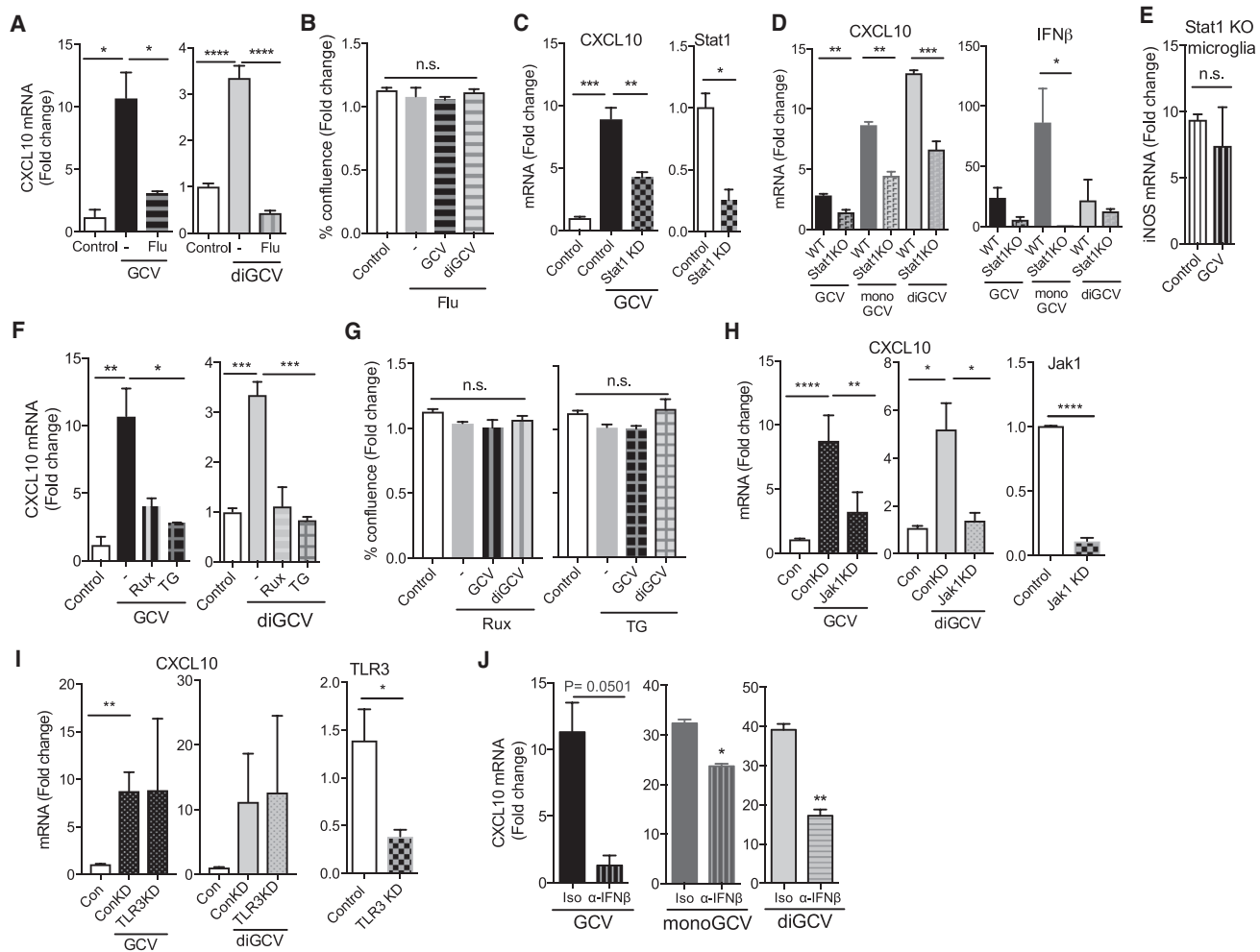


Figure 3. Jak-Stat Signaling through IFN β Is Required for Ganciclovir Activity

(A and B) BV-2 cells were treated with GCV or diGCV along with 10 μ M fludarabine (Flu) for 24 hr. mRNA fold change was analyzed by qRT-PCR (A), and viability was assessed using an automated cell counter (B).

(C) BV-2 cells were transfected with control or Stat1 siRNA for 24 hr and then stimulated with GCV for another 24 hr. CXCL10 mRNA fold change (left) and efficiency of knockdown (right) are shown.

(D and E) Primary microglia from wild-type (WT) and Stat1 knockout (Stat1 KO) mice were treated with GCV, monoGCV, or diGCV for 6 hr (D) or with IFN γ /LPS with or without GCV for 24 hr (E). The indicated transcripts were analyzed by qRT-PCR.

(F and G) BV-2 cells were treated with GCV or diGCV along with 1 μ M ruxolitinib (Rux) or TG101348 (TG) for 24 hr. mRNA (F) and viability (G) are shown.

(H and I) BV-2 cells were transfected with control, Jak1 (H), or TLR3 (I) siRNA for 24 hr and then stimulated with GCV or diGCV for another 24 hr. CXCL10 mRNA fold change (left) and efficiency of knockdown (right) are shown.

(J) BV-2 cells were treated with GCV, monoGCV, or diGCV with anti-IFN β antibody (α -IFN β) or isotype (Iso) control for 4 hr, and mRNA was quantified.

Drug treatments were performed with 200 μ M unless otherwise noted. Statistical tests: one-way ANOVA followed by Dunnett's multiple comparison test (A–C and F–I) or unpaired Student's t test (C, right; D and H, right; I, right; and J). Error bars represent mean + SEM from 3 (cell lines) or 2 (primary cells) independent experiments. * p < 0.05, ** p < 0.01, *** p < 0.001, **** p < 0.0001.

detectable in other CNS cell types (Figure 5B; Figure S4). Interestingly, EAE induction led to a dramatic increase in STING expression in Iba1⁺ myeloid cells as well as in Tmem119⁺ microglia, and GCV reversed this phenotype almost completely (Figure 5B). We next asked if STING was required for the therapeutic effects of GCV in the EAE mouse model. As we reported previously (Ding et al., 2014), GCV drastically reduced disease severity in WT mice in three independent experiments (Figure 5C), lowering disease incidence

by 60%–70% (Figure 5D) and lethality from 20% to 0% (Figure 5E). Although mice lacking STING showed a very similar disease course as WT mice (Figures 5C–5E), GCV failed to significantly reduce disease severity (Figure 5C), incidence (Figure 5D), and lethality (Figure 5E) in STING^{gt/gt} mice at advanced stages of the disease. However, during the early phase of disease, GCV only partially ameliorated EAE, possibly because of compensatory mechanisms and other unknown complexities of EAE progression in STING^{gt/gt}

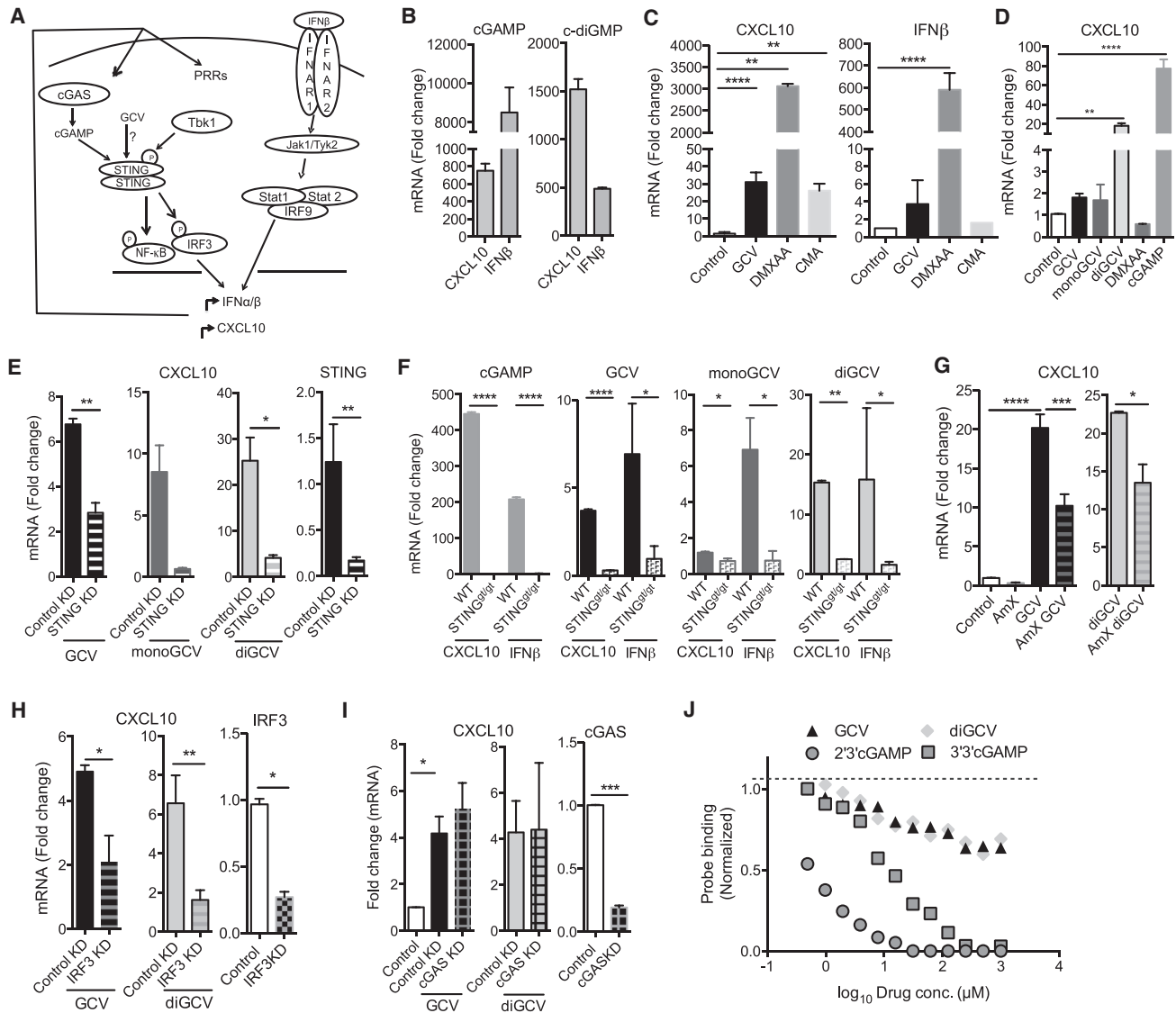


Figure 4. The STING Pathway Is Required for Ganciclovir Activity in Microglia

(A) Schematic showing that STING induces IFN β via Tbk1 and IRF3 and that further activation of Jak/Stat signaling activates the antiviral interferon response. PRR, pattern recognition receptor.
 (B–D) BV-2 (B and C) and THP-1 (D) cells were treated with the drugs for 24 hr and 8 hr, respectively, and the indicated transcripts were quantified.
 (E) STING was knocked down in BV-2 cells using siRNA for 24 hr. Cells were then stimulated with GCV, monoGCV, or diGCV for an additional 24 hr. Fold change in CXCL10 mRNA (left) and efficiency of STING knockdown (right) are shown.
 (F) Primary microglia from WT or STING^{gt/gt} mice were treated with cGAMP, GCV, monoGCV, and diGCV for 6 hr, and the indicated transcripts were analyzed. mRNA fold change was determined by qRT-PCR.
 (G) BV-2 cells were treated with GCV or diGCV along with the Tbk1 inhibitor amlexanox (AmX, 1 μ M) for 24 hr, and CXCL10 mRNA was quantified.
 (H and I) IRF3 (H) or cGAS (I) was knocked down in BV-2 cells using siRNA for 24 hr. Cells were then stimulated with GCV or diGCV for an additional 24 hr. Fold change in CXCL10 mRNA (left) and efficiency of knockdown (right) are shown. GCV and diGCV treatments were performed with 200 μ M drugs.
 (J) Competition binding assay using 500 pM ³⁵S-labeled 2'3'-cGAMP probe, showing that 2'3'-cGAMP and 3'3'-cGAMP, but not GCV and diGCV, dose-dependently compete with 2'3'-cGAMP for binding to 100 nM mouse STING (mSTING).
 Statistical tests: one-way ANOVA followed by Dunnett's multiple comparison test (C and D) or unpaired Student's t test (E–I). mRNA fold change was determined by qRT-PCR. Error bars represent mean + SEM from 3 (cell lines) or 2 (primary cells) independent experiments. * p < 0.05, ** p < 0.01, *** p < 0.001, **** p < 0.0001.

mice. It was shown that STING^{gt/gt} mice exhibit attenuated EAE development compared with WT mice (Lemos et al., 2014). We hypothesize that the intermediate effect on EAE scores by GCV in STING^{gt/gt} mice is due to this slow and

possibly altered EAE pathology. In support of this, STING^{gt/gt} mice with EAE show higher numbers of proliferating cells overall (Figure 5F), proliferating T cells (Figure 5K; Figure S6E), and activated microglia (Figure 6C).

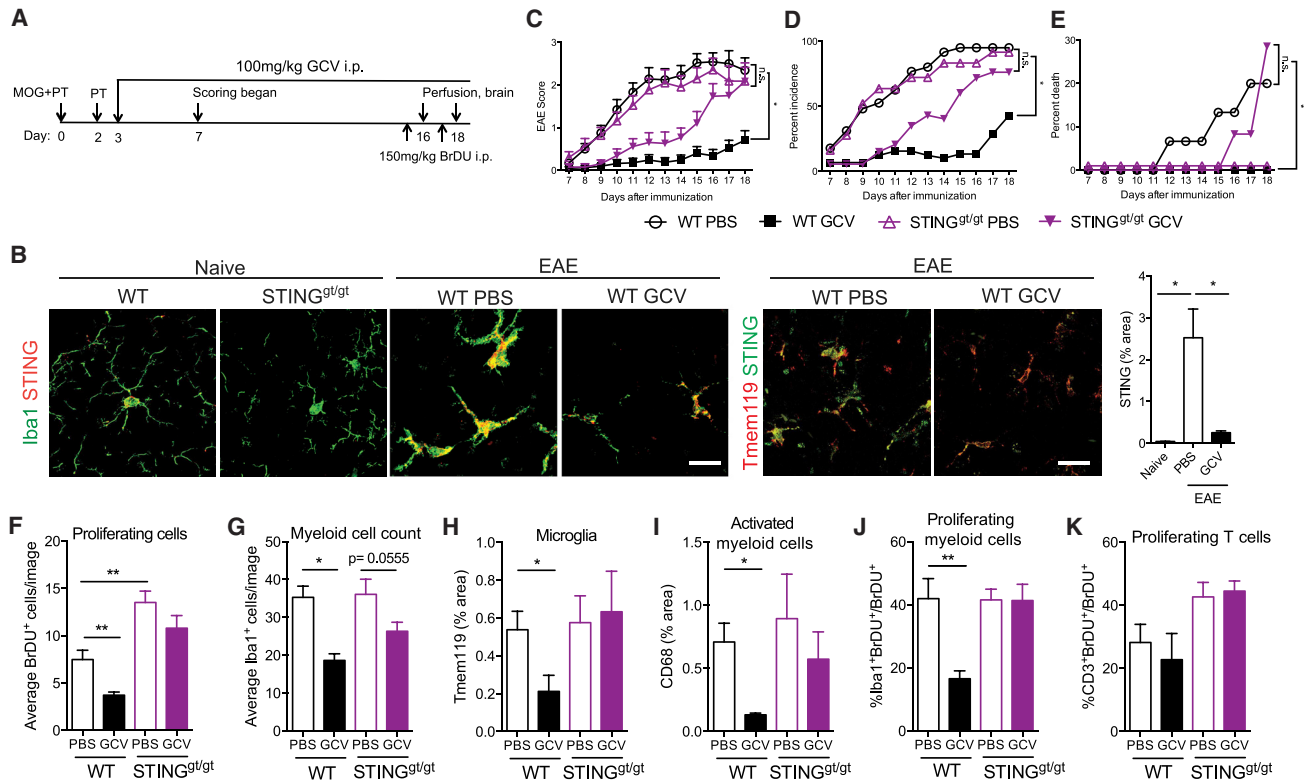


Figure 5. STING Is Required for Inhibition of Inflammation in EAE by Ganciclovir

(A) Schematic showing the experimental design. (B) Representative merged images showing STING expression in Iba1⁺ and Tmem119⁺ cells in the hippocampus (naive) or cerebella (EAE) of mice. The bar graph shows quantification of STING expression. Scale bar, 20 μ m. (C–E) EAE score (C), percent incidence (D), and percent death (E) are depicted for the indicated groups. Data are cumulative of 3 independent experiments (n = 25–32 mice/group). (F–K) Quantification of the average number of BrdU⁺ proliferating cells (F), Iba1⁺ myeloid cells (G), Tmem119 expression (H), CD68 expression (I), percent Iba1⁺BrdU⁺ proliferating myeloid cells (J), and CD3⁺BrdU⁺ proliferating T cells (K). For histology, n = 6–10 mice/group. Error bars represent mean + SEM. Statistical tests: two-way ANOVA followed by Sidak's multiple comparisons test between the indicated groups. *p < 0.05, **p < 0.01, ***p < 0.001, ****p < 0.0001.

Consistent with our published data (Ding et al., 2014), GCV significantly decreased the numbers of bromodeoxyuridine (BrdU)⁺ and PCNA⁺ proliferating cells (Figure 5F and S5), Iba1⁺ myeloid cells (Figure 5G), Iba1⁺BrdU⁺ and Iba1⁺PCNA⁺ proliferating myeloid cells (Figure 5J; Figure S5) but did not change CD3⁺BrdU⁺ proliferating T cells (Figure 5K) in cerebella and spinal cords (Figure S6) of WT mice with EAE. GCV treatment did not increase the number of cleaved caspase-3⁺ cells (Figure S7), suggesting that the inhibition of myeloid proliferation by GCV was not due to induction of apoptosis. Additionally, GCV-treated WT EAE mice showed reduced expression of the microglia-specific marker Tmem119 (Figure 5H; Figures S4B and S8) and the microglial activation marker CD68 (Figure 5I; Figure S8). In stark contrast, and in agreement with the pre-clinical data above, GCV-treated STING^{gt/gt} mice with EAE showed no reduction in overall cell proliferation (Figure 5F; Figures S5 and S6), Tmem119 expression (Figure 5H), myeloid cell activation (Figure 5I), proliferating myeloid cells (Figure 5J; Figures S5 and S6), or T cells (Figure 5K; Figure S6).

To deduce whether this effect of GCV on EAE was due to inhibition of infiltrating myeloid cells or resident CNS microglia, we isolated CD11b⁺ myeloid cells from the cerebella of WT and STING^{gt/gt} mice, with or without EAE, and analyzed CD45 immunoreactivity (Figure 6). GCV treatment reduced total CD45^{hi} (Figure 6A) and CD11b⁺CD45^{hi} (Figure 6B) activated myeloid cells as well as Tmem119⁺CD45^{hi} activated microglia (Figure 6C) in WT EAE but not in STING^{gt/gt} mice, suggesting that GCV exerts its effects on both the infiltrating (Tmem119⁻, CD45^{hi}) as well as resident microglia in the CNS (Tmem119⁺). Interestingly, STING^{gt/gt} mice with EAE had twice as many proliferating cells as WT mice (Figure 5F), and showed a trend toward increasing overall T cell proliferation (Figure 5K), and CD68 and CD45^{hi} immunoreactivity (Figures 5I and 6C), suggesting an altered EAE pathology in these mice.

Finally, to elaborate these anti-inflammatory effects of GCV, we isolated CD11b⁺Tmem119⁺ microglia (Figure 7A) from GCV-treated WT and STING^{gt/gt} mice with EAE and analyzed them by RNA sequencing (RNA-seq). Unsupervised clustering of significantly changed genes segregated

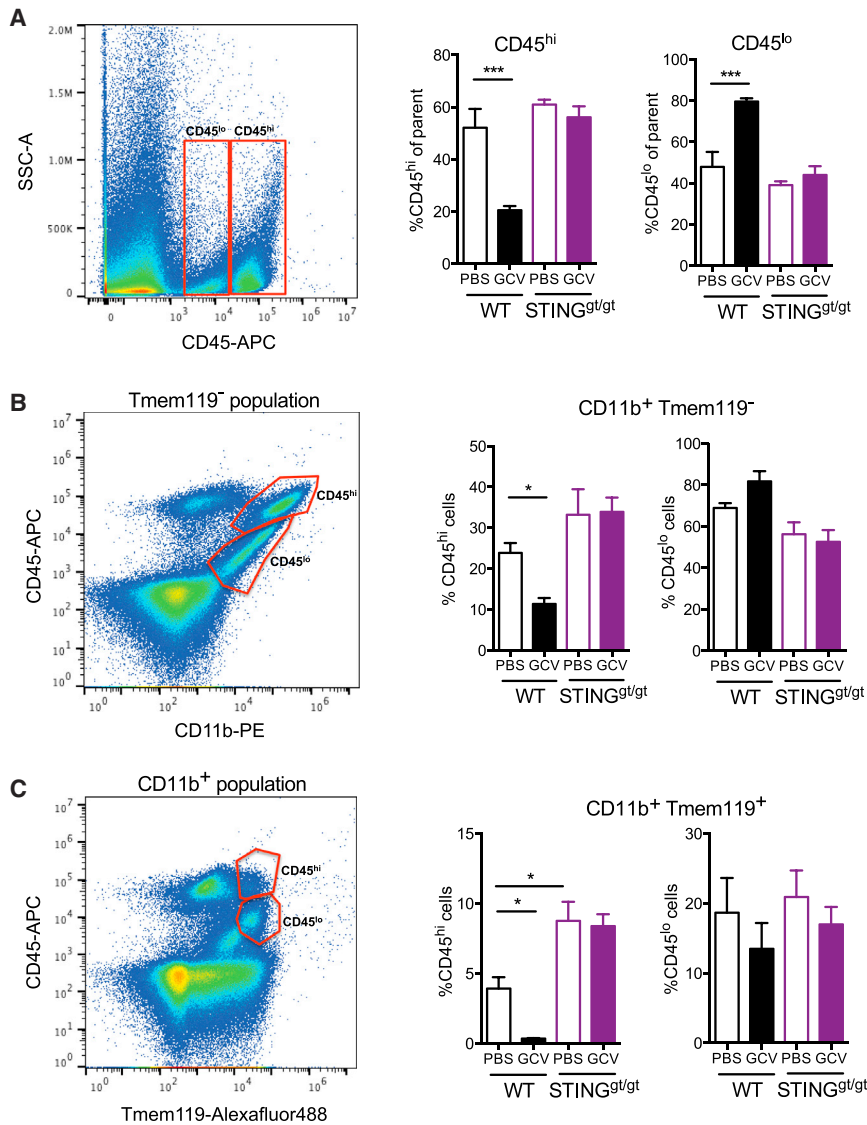


Figure 6. Ganciclovir Reduces CD45^{hi} Myeloid and Microglial Cells in WT but Not STING^{gt/gt} Mice with EAE

(A–C) Flow cytometry analysis of CD11b, CD45, and Tmem119 in isolated microglia from the cerebella of WT and STING^{gt/gt} EAE mice treated with GCV. Left: representative flow dot plots. Right: quantification of CD45^{hi} and CD45^{lo} populations (A) in CD11b⁺ Tmem119⁻ cells (B) and CD11b⁺ Tmem119⁺ microglia (C). n = 3–4 mice/group. Error bars represent mean + SEM. Statistical tests: two-way ANOVA followed by Sidak's multiple comparisons test between the indicated groups. *p < 0.05, **p < 0.01, ***p < 0.001, ****p < 0.0001.

GCV-treated WT microglia from the other groups (Figures 7B and 7C). The most significant differences were found between WT PBS- and GCV-treated microglia (Table S2), and they were all STING-dependent (Figure 7D), supporting our finding that GCV requires STING to regulate microglial activity. The most significantly modulated genes by GCV in microglia from WT mice with EAE (Figure 7E) are known to be associated with inflammation (Alox5, Faim3, Ctsb, Lyz1, Clec2i, and Apoe), small-molecule transport (Sidt1, Fabp5, and Slc25a31), and G-protein-coupled receptors (F2r12). Inflammatory response was the most significant GO term associated with GCV versus PBS WT microglia from mice with EAE (Figure 7F). Interestingly, some genes (e.g., Ctsb, Apoe, and Lyz1) that were significantly downregulated with GCV treatment were recently described as disease-associated microglia (DAM) genes in microglia from Alzheimer's and Amyotrophic Lateral Sclerosis (ALS) mouse models (Keren-Shaul et al., 2017). We compared DAM genes

IFNs and results in downregulation of disease-associated genes in a STING-dependent way, reducing inflammation.

DISCUSSION

In aggregate, these studies show that GCV reduces EAE in a STING-dependent fashion similar to DNA nanoparticles, which were recently shown to attenuate EAE (Lemos et al., 2014). STING is highly regulated in microglia *in vivo*, and activation of the STING pathway reduces microglial reactivity and the neuro-inflammatory disease EAE. Because excessive IFN production is linked to interferonopathies such as STING-associated vasculopathy with onset in infancy (SAVI) and Aicardi-Goutières syndrome (Rodero and Crow, 2016), it will be important to find the optimal therapeutic levels to activate the STING pathway in a beneficial way.

Ganciclovir is a widely used antiviral drug and a close analog of acyclovir, the first successful antiviral drug, described in 1977 to

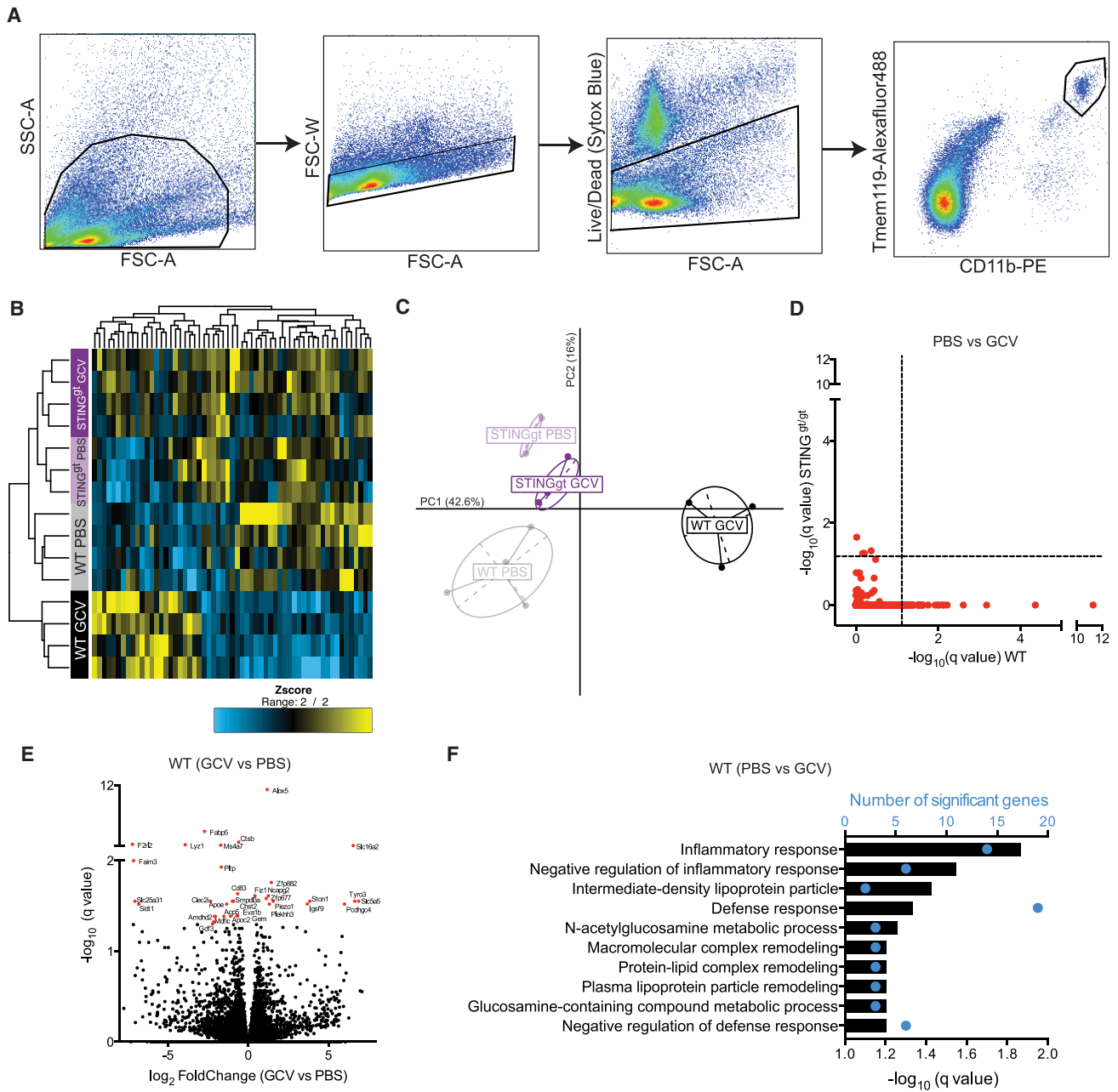


Figure 7. RNA-Seq of Microglia from Mice with EAE Shows that Ganciclovir Inhibits Inflammation in a STING-Dependent Manner

(A) Flow sorting scheme for isolation of CD11b⁺Tmem119⁺ cells from mice with EAE.
 (B) Heatmap showing significantly changed genes ($q < 0.05$) between at least two groups ($n = 3-4$ mice/group).
 (C) Principal-component analysis (PCA) using significant genes.
 (D) $-\log_{10}$ q value plots from WT and STING^{gt/gt} PBS versus GCV differential expression comparison. The dashed line indicates $q = 0.05$.
 (E) Volcano plot showing differentially expressed genes in WT GCV versus WT PBS microglia from mice with EAE.
 (F) GO terms associated with the top 100 differentially expressed genes ranked by q value in WT PBS versus GCV comparison.

exploit viral thymidine kinase activity and inhibit viral replication (Eliou et al., 1977). After decades of highly effective use in humans, our study uncovered a remarkable non-canonical activity of GCV, but not acyclovir, that involves the innate immune receptor STING and a stereotypical cellular antiviral program. We

show that GCV can exhibit dual function in microglia (Figure S10): in the naive state, GCV induces microglia to be “primed”; on the other hand, GCV reduces inflammation in active microglia. We propose that GCV pushes microglia toward a primed state. This multi-modality of GCV is unique and may, in part, be

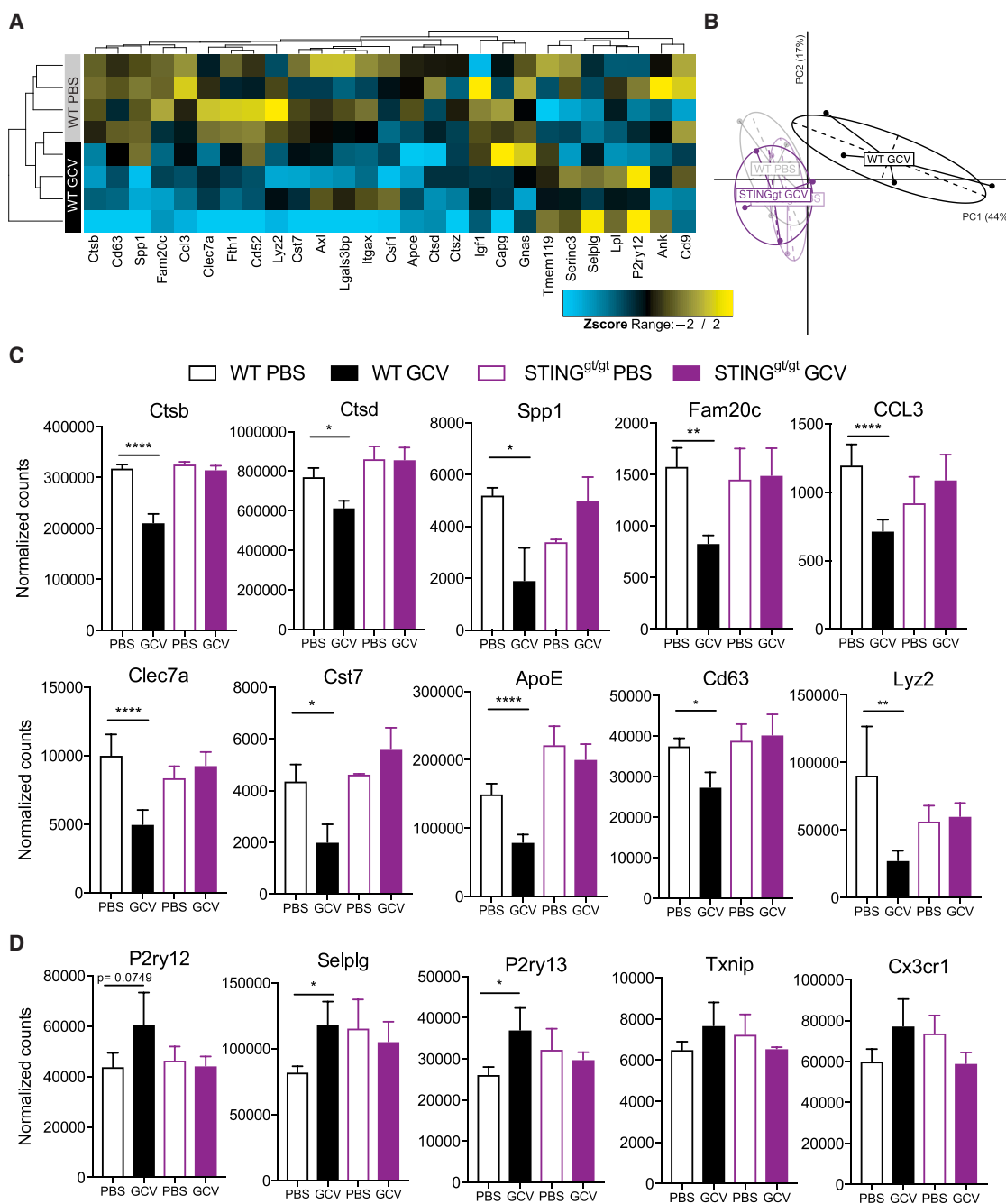


Figure 8. Ganciclovir Treatment Reduces the Expression of Top Disease-Associated Genes in Microglia from Mice with EAE

(A) Heatmap showing differential expression of top disease-associated microglia genes in WT PBS versus GCV groups. The genes with $-\log_{10}(p \text{ value}) > 20$ for homeostatic to DAM (Alzheimer's disease [AD] and ALS) comparisons are represented ($n = 27$).

(B) PCA of top disease-associated microglia genes, showing distinct clustering of GCV-treated WT microglia.

(C and D) Individual plots of normalized counts from RNA-seq data, showing downregulation of disease-associated inflammatory genes (C) and an increase in homeostatic genes (D) by GCV in WT but not STING^{gt/gt} microglia.

Error bars represent mean + SEM. Statistical tests: differential expression analysis based on the negative binomial distribution using DESeq2. * $p < 0.05$, ** $p < 0.01$, *** $p < 0.001$, **** $p < 0.0001$.

responsible for the continued strong success of GCV (and its pro-drug valganciclovir), in spite of many newer antiviral drugs. Lower doses of GCV elicited little to no effect in CNS demyelin-

ation and viral disease models in mice (Skripuletz et al., 2015), suggesting that appropriate dosing is necessary for the novel properties observed here. Alternatively, it is also possible that

GCV does not cross the blood-brain barrier or is functional specifically in the EAE mouse model.

Because of its growing relevance not only in anti-viral immune responses but possibly in sensing mitochondrial damage as well (West et al., 2015), STING has become an attractive target for drug development itself (He et al., 2015). In addition, mutations in STING are associated with vascular and pulmonary syndrome (Liu et al., 2014) and other autoimmune diseases (Jeremiah et al., 2014; Sharma et al., 2015), STING-IRF3 stress is associated with alcoholic liver disease (Petrasek et al., 2013), and haploinsufficiency in the STING activating kinase Tbk1 is associated with ALS and frontotemporal dementia (FTD) (Freischmidt et al., 2015; Pottier et al., 2015). Our findings that GCV, and GCV dimers in particular, activate a type I interferon response in a STING-dependent way and reduce microglial proliferation and neuroinflammation *in vivo* open the possibility to develop a new class of drugs to treat neurodegenerative and related diseases where neuroinflammation has been implicated.

STAR★METHODS

Detailed methods are provided in the online version of this paper and include the following:

- KEY RESOURCES TABLE
- CONTACT FOR REAGENT AND RESOURCE SHARING
- EXPERIMENTAL MODEL AND SUBJECT DETAILS
 - EAE induction and analysis
 - Cell culture
 - Primary microglia and iMGL culture
- METHOD DETAILS
 - RNA preparation and quantitative real time PCR
 - siRNA knockdown
 - Tissue preparation, histology and imaging
 - Flow cytometry
 - STING binding assay
 - RNA sequencing
- QUANTIFICATION AND STATISTICAL ANALYSIS
 - RNA-seq differential expression
 - Gene Ontology (GO) analysis
- DATA AND SOFTWARE AVAILABILITY

SUPPLEMENTAL INFORMATION

Supplemental Information includes ten figures and three tables and can be found with this article online at <https://doi.org/10.1016/j.neuron.2017.11.032>.

ACKNOWLEDGMENTS

We thank Dr. Jian Luo, Dr. Hui Zhang, Dr. Mike Betley, Jadon Shen, and Betty Chang for experimental support and members of the Wyss-Coray lab for helpful discussions and reading of the manuscript. We thank Mariko Bennett and Ben Barres for providing Tmem119 antibodies. This work was funded by a Bluefield Project to Cure Frontotemporal Dementia postdoctoral fellowship (to V.M.), the Department of Veterans Affairs (IO1 RX001218 to T.W.-C.), and the National Institute on Aging (AG045034 to T.W.-C.). Based on this study, V.M., R.B., H.A.L. and T.W.-C. were issued US patent number 9,809,597.

AUTHOR CONTRIBUTIONS

V.M. and T.W.-C. conceptualized and designed the study, analyzed and interpreted data, and wrote the manuscript. V.M., R.T.V., L.N.B., M.Z., D.D., K.N.M., S.E.M., E.M.A., and L.L. acquired the data. R.B. and H.A.L. designed and produced the new GCV derivatives. B.L. analyzed RNA-seq data. M.B.-J. provided iMGLs. All authors reviewed the manuscript.

DECLARATION OF INTERESTS

The authors declare no competing interests.

Received: March 2, 2017

Revised: September 29, 2017

Accepted: November 17, 2017

Published: December 20, 2017

REFERENCES

- Abud, E.M., Ramirez, R.N., Martinez, E.S., Healy, L.M., Nguyen, C.H.H., Newman, S.A., Yeromin, A.V., Scarfone, V.M., Marsh, S.E., Fimbres, C., et al. (2017). iPSC-derived human microglia-like cells to study neurological diseases. *Neuron* 94, 278–293.e9.
- Ahn, J., Konno, H., and Barber, G.N. (2015). Diverse roles of STING-dependent signaling on the development of cancer. *Oncogene* 34, 5302–5308.
- Alexa, A., and Rahnenfuhrer, J. (2010). topGO: enrichment analysis for gene ontology. R package version 2.16.0.
- Andrews, S. (2010). FastQC: a quality control tool for high throughput sequence data (Babraham Bioinformatics).
- Barber, G.N. (2015). STING: infection, inflammation and cancer. *Nat. Rev. Immunol.* 15, 760–770.
- Baruch, K., Deczkowska, A., David, E., Castellano, J.M., Miller, O., Kertser, A., Berkutski, T., Barnett-Izhaki, Z., Bezalel, D., Wyss-Coray, T., et al. (2014). Aging. Aging-induced type I interferon response at the choroid plexus negatively affects brain function. *Science* 346, 89–93.
- Benjamini, Y., and Hochberg, Y. (1995). Controlling the false discovery rate: a practical and powerful approach to multiple testing. *J. R. Stat. Soc. B* 57, 289–300.
- Blasi, E., Barluzzi, R., Bocchini, V., Mazzolla, R., and Bistoni, F. (1990). Immortalization of murine microglial cells by a v-raf/v-myc carrying retrovirus. *J Neuroimmunol.* 27, 229–237.
- Burdette, D.L., Monroe, K.M., Sotelo-Troha, K., Iwig, J.S., Eckert, B., Hyodo, M., Hayakawa, Y., and Vance, R.E. (2011). STING is a direct innate immune sensor of cyclic di-GMP. *Nature* 478, 515–518.
- Cavlar, T., Deimling, T., Ablasser, A., Hopfner, K.P., and Hornung, V. (2013). Species-specific detection of the antiviral small-molecule compound CMA by STING. *EMBO J.* 32, 1440–1450.
- Chin, K.H., Tu, Z.L., Su, Y.C., Yu, Y.J., Chen, H.C., Lo, Y.C., Chen, C.P., Barber, G.N., Chuah, M.L., Liang, Z.X., and Chou, S.H. (2013). Novel c-di-GMP recognition modes of the mouse innate immune adaptor protein STING. *Acta Crystallogr. D Biol. Crystallogr.* 69, 352–366.
- Conlon, J., Burdette, D.L., Sharma, S., Bhat, N., Thompson, M., Jiang, Z., Rathinam, V.A., Monks, B., Jin, T., Xiao, T.S., et al. (2013). Mouse, but not human STING, binds and signals in response to the vascular disrupting agent 5,6-dimethylxanthone-4-acetic acid. *J. Immunol.* 190, 5216–5225.
- Deczkowska, A., Baruch, K., and Schwartz, M. (2016). Type I/II Interferon Balance in the Regulation of Brain Physiology and Pathology. *Trends Immunol.* 37, 181–192.
- Ding, Z., Mathur, V., Ho, P.P., James, M.L., Lucin, K.M., Hoehne, A., Alabsi, H., Gambhir, S.S., Steinman, L., Luo, J., and Wyss-Coray, T. (2014). Antiviral drug ganciclovir is a potent inhibitor of microglial proliferation and neuroinflammation. *J. Exp. Med.* 211, 189–198.

- Dobin, A., Davis, C.A., Schlesinger, F., Drenkow, J., Zaleski, C., Jha, S., Batut, P., Chaisson, M., and Gingeras, T.R. (2013). STAR: ultrafast universal RNA-seq aligner. *Bioinformatics* 29, 15–21.
- Dray, S.p., and Dufour, A.-B.a. (2007). The ade4 package: implementing the duality diagram for ecologists. *J. Stat. Softw.* 22, 1–20.
- Ejlertskov, P., Hultberg, J.G., Wang, J., Carlsson, R., Ambjørn, M., Kuss, M., Liu, Y., Porcu, G., Kolkova, K., Friis Rundsten, C., et al. (2015). Lack of Neuronal IFN- β -IFNAR Causes Lewy Body- and Parkinson's Disease-like Dementia. *Cell* 163, 324–339.
- Eliou, G.B., Furman, P.A., Fyfe, J.A., de Miranda, P., Beauchamp, L., and Schaeffer, H.J. (1977). Selectivity of action of an antiherpetic agent, 9-(2-hydroxyethoxymethyl) guanine. *Proc. Natl. Acad. Sci. USA* 74, 5716–5720.
- Faulds, D., and Heel, R.C. (1990). Ganciclovir. A review of its antiviral activity, pharmacokinetic properties and therapeutic efficacy in cytomegalovirus infections. *Drugs* 39, 597–638.
- Food and Drug Administration (2005). Guidance for industry on estimating the maximum safe starting dose in initial clinical trials for therapeutics in adult healthy volunteers. <https://www.federalregister.gov/documents/2005/07/22/05-14456/guidance-for-industry-on-estimating-the-maximum-safe-starting-dose-in-initial-clinical-trials-for>.
- Frank, D.A., Mahajan, S., and Ritz, J. (1999). Fludarabine-induced immunosuppression is associated with inhibition of STAT1 signaling. *Nat. Med.* 5, 444–447.
- Freischmidt, A., Wieland, T., Richter, B., Ruf, W., Schaeffer, V., Müller, K., Marroquin, N., Nordin, F., Hübers, A., Weydt, P., et al. (2015). Haploinsufficiency of TBK1 causes familial ALS and fronto-temporal dementia. *Nat. Neurosci.* 18, 631–636.
- Fu, J., Kanne, D.B., Leong, M., Glickman, L.H., McWhirter, S.M., Lemmens, E., Mechette, K., Leong, J.J., Lauer, P., Liu, W., et al. (2015). STING agonist formulated cancer vaccines can cure established tumors resistant to PD-1 blockade. *Sci. Transl. Med.* 7, 283ra52.
- Gao, P., Ascano, M., Zillinger, T., Wang, W., Dai, P., Serganov, A.A., Gaffney, B.L., Shuman, S., Jones, R.A., Deng, L., et al. (2013). Structure-function analysis of STING activation by c[G(2',5')pA(3',5')p] and targeting by antiviral DMXAA. *Cell* 154, 748–762.
- Glass, C.K., Saijo, K., Winner, B., Marchetto, M.C., and Gage, F.H. (2010). Mechanisms underlying inflammation in neurodegeneration. *Cell* 140, 918–934.
- Group, T.I.M.S.S.; The IFNB Multiple Sclerosis Study Group (1993). Interferon beta-1b is effective in relapsing-remitting multiple sclerosis. I. Clinical results of a multicenter, randomized, double-blind, placebo-controlled trial. *Neurology* 43, 655–661.
- He, S., Mao, X., Sun, H., Shirakawa, T., Zhang, H., and Wang, X. (2015). Potential therapeutic targets in the process of nucleic acid recognition: opportunities and challenges. *Trends Pharmacol. Sci.* 36, 51–64.
- Hornung, V., Hartmann, R., Ablasser, A., and Hopfner, K.P. (2014). OAS proteins and cGAS: unifying concepts in sensing and responding to cytosolic nucleic acids. *Nat. Rev. Immunol.* 14, 521–528.
- Ishikawa, H., and Barber, G.N. (2008). STING is an endoplasmic reticulum adaptor that facilitates innate immune signaling. *Nature* 455, 674–678.
- Ishikawa, H., Ma, Z., and Barber, G.N. (2009). STING regulates intracellular DNA-mediated, type I interferon-dependent innate immunity. *Nature* 461, 788–792.
- Jeremiah, N., Neven, B., Gentili, M., Callebaut, I., Maschalidi, S., Stolzenberg, M.C., Goudin, N., Frémond, M.L., Nitschke, P., Molina, T.J., et al. (2014). Inherited STING-activating mutation underlies a familial inflammatory syndrome with lupus-like manifestations. *J. Clin. Invest.* 124, 5516–5520.
- Keren-Shaul, H., Spinrad, A., Weiner, A., Matcovitch-Natan, O., Dvir-Szternfeld, R., Ulland, T.K., David, E., Baruch, K., Lara-Astaiso, D., Toth, B., et al. (2017). A unique microglia type associated with restricting development of alzheimer's disease. *Cell* 169, 1276–1290.e17.
- Kunis, G., Baruch, K., Rosenzweig, N., Kertser, A., Miller, O., Berkutzki, T., and Schwartz, M. (2013). IFN- γ -dependent activation of the brain's choroid plexus for CNS immune surveillance and repair. *Brain* 136, 3427–3440.
- Lemos, H., Huang, L., Chandler, P.R., Mohamed, E., Souza, G.R., Li, L., Pacholczyk, G., Barber, G.N., Hayakawa, Y., Munn, D.H., and Mellor, A.L. (2014). Activation of the STING adaptor attenuates experimental autoimmune encephalitis. *J. Immunol.* 192, 5571–5578.
- Lewis, N.D., Hill, J.D., Juchem, K.W., Stefanopoulos, D.E., and Modis, L.K. (2014). RNA sequencing of microglia and monocyte-derived macrophages from mice with experimental autoimmune encephalomyelitis illustrates a changing phenotype with disease course. *J. Neuroimmunol.* 277, 26–38.
- Li, L., Yin, Q., Kuss, P., Maliga, Z., Millán, J.L., Wu, H., and Mitchison, T.J. (2014). Hydrolysis of 2'3'-cGAMP by ENPP1 and design of nonhydrolyzable analogs. *Nat. Chem. Biol.* 10, 1043–1048.
- Liddel, S.A., Guttenplan, K.A., Clarke, L.E., Bennett, F.C., Bohlen, C.J., Schirmer, L., Bennett, M.L., Münch, A.E., Chung, W.S., Peterson, T.C., et al. (2017). Neurotoxic reactive astrocytes are induced by activated microglia. *Nature* 541, 481–487.
- Littler, E., Stuart, A.D., and Chee, M.S. (1992). Human cytomegalovirus UL97 open reading frame encodes a protein that phosphorylates the antiviral nucleoside analogue ganciclovir. *Nature* 358, 160–162.
- Liu, M., Guo, S., and Stiles, J.K. (2011). The emerging role of CXCL10 in cancer (Review). *Oncol. Lett.* 2, 583–589.
- Liu, Y., Jesus, A.A., Marrero, B., Yang, D., Ramsey, S.E., Sanchez, G.A.M., Tenbrock, K., Wittkowski, H., Jones, O.Y., Kuehn, H.S., et al. (2014). Activated STING in a vascular and pulmonary syndrome. *N. Engl. J. Med.* 371, 507–518.
- Love, M.I., Huber, W., and Anders, S. (2014). Moderated estimation of fold change and dispersion for RNA-seq data with DESeq2. *Genome Biol.* 15, 550.
- Matthews, T., and Boehme, R. (1988). Antiviral activity and mechanism of action of ganciclovir. *Rev. Infect. Dis.* 10 (Suppl 3), S490–S494.
- Okabe, Y., Sano, T., and Nagata, S. (2009). Regulation of the innate immune response by threonine-phosphatase of Eyes absent. *Nature* 460, 520–524.
- Petrasek, J., Iracheta-Velhe, A., Csak, T., Satishchandran, A., Kodys, K., Kurt-Jones, E.A., Fitzgerald, K.A., and Szabo, G. (2013). STING-IRF3 pathway links endoplasmic reticulum stress with hepatocyte apoptosis in early alcoholic liver disease. *Proc. Natl. Acad. Sci. USA* 110, 16544–16549.
- Pottier, C., Bieniek, K.F., Finch, N., van de Vorst, M., Baker, M., Perkersen, R., Brown, P., Ravenscroft, T., van Blitterswijk, M., Nicholson, A.M., et al. (2015). Whole-genome sequencing reveals important role for TBK1 and OPTN mutations in frontotemporal lobar degeneration without motor neuron disease. *Acta Neuropathol.* 130, 77–92.
- Prantner, D., Perkins, D.J., Lai, W., Williams, M.S., Sharma, S., Fitzgerald, K.A., and Vogel, S.N. (2012). 5,6-Dimethylxanthone-4-acetic acid (DMXAA) activates stimulator of interferon gene (STING)-dependent innate immune pathways and is regulated by mitochondrial membrane potential. *J. Biol. Chem.* 287, 39776–39788.
- Rodero, M.P., and Crow, Y.J. (2016). Type I interferon-mediated monogenic autoinflammation: The type I interferonopathies, a conceptual overview. *J. Exp. Med.* 213, 2527–2538.
- Sauer, J.D., Sotelo-Troha, K., von Molte, J., Monroe, K.M., Rae, C.S., Brubaker, S.W., Hyodo, M., Hayakawa, Y., Woodward, J.J., Portnoy, D.A., and Vance, R.E. (2011). The N-ethyl-N-nitrosourea-induced Goldenticket mouse mutant reveals an essential function of Sting in the in vivo interferon response to *Listeria monocytogenes* and cyclic dinucleotides. *Infect. Immun.* 79, 688–694.
- Schoggins, J.W., Wilson, S.J., Panis, M., Murphy, M.Y., Jones, C.T., Bieniasz, P., and Rice, C.M. (2011). A diverse range of gene products are effectors of the type I interferon antiviral response. *Nature* 472, 481–485.
- Sharma, S., Campbell, A.M., Chan, J., Schattgen, S.A., Orlowski, G.M., Nayar, R., Huyler, A.H., Nündel, K., Mohan, C., Berg, L.J., et al. (2015). Suppression of

- systemic autoimmunity by the innate immune adaptor STING. *Proc. Natl. Acad. Sci. USA* *112*, E710–E717.
- Skripuletz, T., Salinas Tejedor, L., Prajeeth, C.K., Hansmann, F., Chhatbar, C., Kucman, V., Zhang, N., Raddatz, B.B., Detje, C.N., Sühs, K.W., et al. (2015). The antiviral drug ganciclovir does not inhibit microglial proliferation and activation. *Sci. Rep.* *5*, 14935.
- Sun, W., Li, Y., Chen, L., Chen, H., You, F., Zhou, X., Zhou, Y., Zhai, Z., Chen, D., and Jiang, Z. (2009). ERS, an endoplasmic reticulum IFN stimulator, activates innate immune signaling through dimerization. *Proc. Natl. Acad. Sci. USA* *106*, 8653–8658.
- Takeuchi, O., and Akira, S. (2010). Pattern recognition receptors and inflammation. *Cell* *140*, 805–820.
- Warnes, G.R., Bolker, B., Bonebakker, L., Gentleman, R., Huber, W., Liaw, A., Lumley, T., Maechler, M., Magnusson, A., Moeller, S., et al. (2016). *gplots: Various R Programming Tools for Plotting Data*. R package version 3.0.1 (The Comprehensive R Archive Network).
- West, A.P., Khoury-Hanold, W., Staron, M., Tal, M.C., Pineda, C.M., Lang, S.M., Bestwick, M., Duguay, B.A., Raimundo, N., MacDuff, D.A., et al. (2015). Mitochondrial DNA stress primes the antiviral innate immune response. *Nature* *520*, 553–557.
- Zhou, T., Georgeon, S., Moser, R., Moore, D.J., Cafisch, A., and Hantschel, O. (2014). Specificity and mechanism-of-action of the JAK2 tyrosine kinase inhibitors ruxolitinib and SAR302503 (TG101348). *Leukemia* *28*, 404–407.

STAR★METHODS

KEY RESOURCES TABLE

REAGENT or RESOURCE	SOURCE	IDENTIFIER
Antibodies		
BrDU	Abcam	Cat# 6326; RRID: AB_305426
Active Caspase 3	Cell Signaling Technologies	Cat# 9661; RRID: AB_2341188
CD11b-PE	BD Biosciences	Cat# 12-0112-82
CD45-APC	BD Biosciences	Cat# 559864
CD68	BioRad	Cat# MCA1957; RRID: AB_2074849
Iba1	Abcam	Cat# ab5076; RRID: AB_2224402
PCNA	Dako	Cat# M0879; RRID: AB_2160651
iNOS/NOS2	BD Biosciences	Cat# 610328; RRID: AB_397718
STING	Cell Signaling Technologies	Cat# 13647
Tmem119 (106-6) Flow	Abcam	Cat# 210405
Tmem119 (28-3) IHC	Abcam	Cat# 209064
Chemicals, Peptides, and Recombinant Proteins		
Ganciclovir	Stanford Health Care Pharmacy	APP Pharmaceuticals Cat#315110
IFN γ	R&D Systems	Cat#575306
LPS	Sigma-Aldrich	Cat#L2880-10MG
Fludarabine	Selleckchem	Cat#S1491
Ruxolitinib	Selleckchem	Cat#S1378
TG-101348	Selleckchem	Cat#S2736
Amlexanox	Tocris Bioscience	Cat#4857/10
monoGCV	this study	N/A
diGCV	this study	N/A
MethylGCV	this study	N/A
ThiolGCV	this study	N/A
DMXAA	Selleckchem	Cat#S1537
CMA	Sigma Aldrich	Cat#17927-250MG
Penciclovir	Sigma Aldrich	Cat#P0035
Acyclovir	Stanford Health Care Pharmacy	APP Pharmaceuticals Cat#302510
Guanine	Sigma Aldrich	Cat#G11950-100G
Guanosine	Sigma Aldrich	Cat#G6752-100G
Ribavirin	Selleckchem	Cat#S2504/50-670-7
Vidarabine	Selleckchem	Cat#S1784/50-101-0115
Foscarnet	Selleckchem	Cat#S3076
Cidofovir	Selleckchem	Cat#S1516/50-791-0
DMEM/ F12	Life Technologies	Cat#11320-033
FBS	Atlanta Biologicals	Cat#S11550H
RPMI-40	Thermo Scientific	Cat#11875-093
β -mercaptoethanol	Thermo Scientific	Cat#21985023
1X TrypLE	Life Technologies	Cat#12605-036
poly-L-lysine hydrobromide, MW70k-150k	Sigma Aldrich	Cat#P6282-5MG
Penicillin/streptomycin	Life Technologies	Cat#15140-122
CD11b magnetic beads	Miltenyi Biotec	Cat#130-049-601
LightCycler 480 SYBR Green I Master Mix	Roche	Cat#04887352001
MOG ₃₅₋₅₅ peptide	Stanford PAN facility	N/A

(Continued on next page)

Continued

REAGENT or RESOURCE	SOURCE	IDENTIFIER
Pertussis Toxin	Fisher	Cat#NC9675592
Phosphate Buffered Saline	Life Technologies	Cat#PHZ1174
BrDU	Sigma Aldrich	Cat#19-160
Avertin (Tribromoethanol)	Sigma Aldrich	Cat#T48402
Paraformaldehyde	Sigma Aldrich	Cat#P6148-1KG
Sucrose	Sigma Aldrich	Cat#S9378
HCl	Sigma Aldrich	Cat#258148
Tri Sodium Citrate	Sigma Aldrich	Cat#S4641
Tween 20	Sigma Aldrich	Cat#P1379
2'3'-cGAMP	Invivogen	Cat#tlrl-nacga23
Methanol	Fisher	Cat#A412-4
HBSS+	Life Technologies	Cat# 14025-092
HBSS-	Life Technologies	Cat#14175-103
1M HEPES	Thermo Scientific	Cat#15630-106
Glucose	Sigma Aldrich	Cat#158968
DnaseI	Fisher	Cat#18068-015
Percoll	Fisher/GE healthcare life sciences	Cat#45001753/17-5445-01
BSA	Sigma-Aldrich	Cat#A7888-50G
EDTA	Thermo Scientific	Cat#15575-020
³⁵ S-labeled 2'3'-cGAMP	Li et al., 2014	N/A
mSTING	Li et al., 2014	N/A
Neural Dissociation Kit	Miltenyi Biotec	Cat#130-092-628
Viromer Blue	Lipocalyx	Cat#VB-01LB-01
Rneasy mini kit	QIAGEN	Cat#74104
SuperScript III First-Strand Synthesis System	Life Technologies	Cat#18080-051
RNeasy Plus Micro kit	QIAGEN	Cat#74004
SMART-seq v4 Ultra Low input RNA kit for sequencing	Takara Bio USA, Inc.	Cat#634892
Agencourt AMPure XP	Beckman Coulter	Cat#68298
Nextera XT DNA library prep kit	Illumina	Cat#FC-131-1024
Critical Commercial Assays		
Griess Reagent System	Promega	Cat#G2930
96.96 Dynamic Array Chip	Fluidigm	Cat#BMK-M-96.96
Celltox green cytotoxicity assay	Promega	Cat# G8741
Experimental Models: Cell Lines		
THP-1	ATCC	Cat#TIB-202; RRID: CVCL_0006
BV2	Blasi et al., 1990	N/A
iCell® Hematopoietic Progenitor Cells	Cellular Dynamics International	Cat # R1094
SMARTpool siGENOME TLR3 siRNA	GE Dharmacon	Cat#M-059850-01-0005
SMARTpool siGENOME Mb21D1 siRNA	GE Dharmacon	Cat#M-055608-01-0005
SMARTpool siGENOME Jak1 siRNA	GE Dharmacon	Cat#M-040117-01-0005
SMARTpool siGENOME STING siRNA	GE Dharmacon	Cat#M-055528-01-0005
SMARTpool siGENOME Stat1 siRNA	GE Dharmacon	Cat#M-058881-02-0005
Experimental Models: Organisms/Strains		
C57BL/6 WT	Jackson Laboratory	Stock No: 000664; RRID:IMSR_JAX:000664
Tk1 KO, B6;129P2-Tk1tm1Vnd/Mmcd	MMRRC	000014-UCD; RRID:MMRRC_000014-UCD
Tmem173 gt/J	Jackson Laboratory	Stock No:017537; RRID:IMSR_JAX:017537
B6.129S(Cg)-Stat1tm1Dlv/J	Jackson Laboratory	Cat#012606; RRID:IMSR_JAX:012606

(Continued on next page)

Continued		
REAGENT or RESOURCE	SOURCE	IDENTIFIER
Oligonucleotides		
Primers for qPCR, see Table S3		
Software and Algorithms		
FlowJo v.10.0	N/A	https://www.flowjo.com/solutions/flowjo
GraphPad Prism v.7	N/A	https://www.graphpad.com/scientific-software/prism/
ZEN 2.0 software	N/A	https://www.zeiss.com/microscopy/us/products/microscope-software/zen-2-core.html
FASTQC (v 0.11.4)	Andrews, 2010	N/A
STAR (v 2.5.1b)	Dobin et al., 2013	N/A
fastX toolkit (v 0.0.14)	N/A	http://hannonlab.cshl.edu/fastx_toolkit/
R DESeq2 package	Love et al., 2014	N/A
ade4	Dray and Dufour, 2007	N/A
gplots	Warnes et al., 2016	N/A
Benjamini and Hochberg approach	Benjamini and Hochberg, 1995	N/A
top GO R package	Alexa and Rahnenfuhrer, 2010	N/A
ImageJ	N/A	https://imagej.nih.gov/ij/
Deposited data		
RNA-seq	This study	GEO: GSE106692
Other		
BD Accuri C6	BD Biosciences	N/A
LSM 700/880	Zeiss	N/A
Lightcycler 480 II	Roche	N/A
Cellavista	Innovatis	N/A
Illumina Novaseq 6000	Novogene	N/A
Advanced Analytical Fragment Analyzer	Stanford PAN facility	N/A
Agilent 2100 Bioanalyzer	Stanford PAN facility	N/A
NanoflexTM 4-IFC Controller	Fluidigm	N/A
BioMark Real-Time PCR System	Fluidigm	N/A
BD FACSAria III	BD Biosciences	N/A

CONTACT FOR REAGENT AND RESOURCE SHARING

Further information and requests for resources and reagents should be directed to the Lead Contact, Tony Wyss-Coray (twc@stanford.edu).

EXPERIMENTAL MODEL AND SUBJECT DETAILS

EAE induction and analysis

EAE was induced in 2-3 months old C57BL/6 wild-type and STING^{gt/gt} female mice as described ([Ding et al., 2014](#)). Briefly, mice were immunized subcutaneously with 200 μ g mouse MOG₃₅₋₅₅ peptide (Stanford PAN facility) emulsified in CFA (200 μ g *M. tuberculosis*, Difco adjuvants, BD) and injected intravenously with 100ng pertussis toxin (List Biological Laboratories) at 0h and 48h of immunization. Mice were weighed and scored for clinical signs of EAE daily: 0, no paralysis; 1, loss of tail tone; 2, hind limb weakness or paresis; 3, hind limb paralysis; 4, hind limb paralysis and forelimb paresis; 5, moribund or dead. When a mouse died from the disease, it was given a score of 5 that day and subsequently removed from scoring. All mice with or without disease are included in the graphs shown. GCV (100mg/kg) or phosphate buffered saline (PBS) vehicle control were intra-peritoneally injected everyday starting 3 days after immunization till the end of the experiment. BrDU (150 mg/kg) was intra-peritoneally injected 1 day before sacrifice. GCV administration in adults and children ranges from a daily oral dose of up to 4g or multiple daily intravenous doses of 5mg/kg ([Faulds and Heel, 1990](#)). In this study, we used GCV concentrations that are used to treat patients in clinic, adjusted with a factor of 12.3 for human to mouse dose conversion ([Food and Drug Administration, 2005](#)), and are below the reported median inhibitory concentration.

Cell culture

BV-2 female mouse microglia-like cells were grown in DMEM + 10% FBS, and THP-1 male human monocyte cells were grown in RPMI-40 + 10% FBS + 0.05mM β -mercaptoethanol at 37°C, 5% CO₂. Adherent cells were split using 1X TrypLE (GIBCO). For cellular assays, cells were treated with the following concentrations of drugs, unless otherwise noted, in DMEM (for BV-2) or RPMI-40 (for THP-1) without serum: 100- 200 μ M ganciclovir, 10ng/ml IFN γ (R&D systems), 100ng/ml LPS (Sigma-Aldrich), 10 μ M Fludarabine (Selleckchem), 1 μ M Ruxolitinib (Selleckchem), 1 μ M TG-101348 (Selleckchem), 1 μ M Amlexanox (Tocris bioscience). Secreted signaling proteins were measured in conditioned culture supernatants from BV-2 cells stimulated with GCV for 24h in the absence of serum using two independent Luminex arrays (Human Immune Monitoring Center, Stanford University and Eve technologies, Canada). Nitrite assay was performed on conditioned culture supernatants of cells stimulated with drugs for 24h using the Griess Reagent System (Promega) according to manufacturer's instructions. To assess cell viability, cell confluence was measured using an automated microscope (Cellvista; Roche). Toxicity was measured using Celltox Green cytotoxicity assay (Promega). All experiments were run in triplicates and replicated at least 3 times with cell lines and at least twice with primary microglia.

Primary microglia and iMGL culture

Mice were housed, bred and handled according to the Institutional Animal Care and Use Committee guidelines. Primary microglia were isolated from 2-3 months old C57BL/6 wild-type male mice forebrains using the neural dissociation kit (P) followed by CD11b magnetic bead enrichment (Miltenyi Biotec) according to manufacturer's protocol. Isolated cells were cultured at a confluent density in DMEM/F12 + 10% FBS + 1% penicillin/streptomycin for 3-4 days before the experiment.

Primary microglia and astrocytes from P0-P3 C57BL/6 mouse pups (male and female) were isolated from cortices, meninges removed and tissue dissociated using a 25-gauge needle. Two cortices were plated on each poly-L-lysine coated T-75 flasks in DMEM/F12 + 10% FBS + 1% penicillin/streptomycin. Microglia and astrocyte co-cultures were maintained for 3 weeks, after which microglia were isolated using CD11b magnetic beads. Isolated microglia were allowed to recover for 1- 2 days and processed for cellular assays.

Human iMGLs were derived from human induced male Hematopoietic Progenitor Cells (iHPCs) as described (Abud et al., 2017). All stem cell work was performed with approval from UC Irvine Human Stem Cell Research Oversight and IBC committees. CD43⁺ human iHPCs (Cellular Dynamics International) were differentiated to iMGLs using differentiation medium for 25 days and matured in maturation medium for additional 3 days as described (Abud et al., 2017). iMGLs were treated with 200 μ M GCV for 24h in iMGL media and processed for RNA or protein extraction.

METHOD DETAILS

RNA preparation and quantitative real time PCR

For standard quantitative real time PCR (qRT-PCR), RNA was isolated from cells using RNeasy mini kit (QIAGEN). DNased RNA was converted to cDNA using SuperScript III reverse transcriptase kit (Life technologies). cDNA was used to quantify specific targets using SYBR green in Roche Lightcycler 480. β -actin or Ubc or both were used as housekeeping genes. Primer sequences were obtained from Harvard PrimerBank (Table S3). Fold change in transcripts was calculated using $\Delta\Delta$ Ct values based on the experimental controls. Figures depict fold change compared to the vehicle treated or untreated cells, unless otherwise noted.

For microfluidic qRT-PCR, a primer-pair panel was designed consisting of 86 microglia and other cell type specific genes + 10 housekeeping genes (Table S1). The experiment was done as described (Liddelow et al., 2017). cDNA was made and pre-amplified from ~100ng RNA using pre-amplification and reverse transcription kits from Fluidigm using the manufacturer's protocol and diluted 1:5 fold. Sample mix and assay mix were made according to manufacturer's instructions and loaded on 96.96 Dynamic Array Chip (Fluidigm). The chip was then loaded and mixed using NanoFlexTM 4-IFC Controller (Fluidigm), followed by processing and data collection on BioMark Real-Time PCR System (Fluidigm). Fold change was calculated using $\Delta\Delta$ Ct as described above.

siRNA knockdown

Smartpool siRNAs for specific targets were bought from Dharmacon and transfected in microglia-like cells using Viromer Blue (Lipocalyx) at a concentration of 50nM according to manufacturer's instructions. After 24h of transfection, cells were treated with drugs for additional 24h and then processed for analysis.

Tissue preparation, histology and imaging

Mice were anesthetized using Avertin (Tribromoethanol) and perfused by cardiac puncture. Hemibrains and spinal cords were extracted, fixed in 4% paraformaldehyde for 48h, cryoprotected in 30% sucrose and then sectioned sagittally or coronally (40 μ m) using a freezing microtome (Leica). Immunohistochemistry was done on 3-4 free-floating sections per mouse, according to standard procedures. Primary antibodies were against BrDU (1:2,000, Abcam), Iba1 (1:1,000; Wako Chemicals USA; 1:1000, Abcam), CD3 (1:1,000, BD Biosciences), Tmem119 (gift from Ben Barres lab), CD68 (1:600, Biorad), PCNA (1:500, Dako) and Cleaved Caspase3 (1:500, Cell Signaling Technologies). Sections were treated in 3M HCl for 30 min at 37°C for BrDU antigen retrieval. Citrate antigen retrieval (pH 6.0) was done at 80°C for 20 minutes for Iba1 (Abcam), PCNA and Cleaved Caspase3. Secondary antibodies were Alexa

Fluor 488, 555, 594, 647 (1:500, Life technologies). Z stacks of images were taken on confocal microscope (Zeiss LSM700/880). Double positive cells were counted and images were analyzed using ImageJ.

Flow cytometry

All procedures were carried out at 4°C. For Figure 6, upon reaching disease score of 2 or more, mice were perfused, cerebella from hemi brains of mice were chopped and homogenized using a Dounce homogenizer in 2ml cold Medium A (HBSS+ 15mM HEPES+0.05% glucose+ 1:500 DnaseI), filtered through 100µm cell strainer, rinsed with 5ml Medium A and centrifuged at 340 g for 5 mins. For myelin removal, the precipitate was resuspended in 25% standard isotonic percoll (25% Percoll in PBS, diluted with Medium A) and centrifuged at 950 g for 20 mins. Precipitated cells were washed with FACS buffer (PBS+1% BSA+2mM EDTA) twice and stained with 1:100 CD11b-PE, 1:100 CD45-APC and 16µg/ml rabbit anti-mouse Tmem119 antibodies (85-5 and 106-6, gifts from Ben Barres lab) for 30 mins at room temperature, followed by 1:500 donkey anti-Rabbit-Alexafluor488. Cells were washed and analyzed on BD AccuriC6 flow cytometer.

For RNA sequencing, EAE was induced as above and mice were sacrificed when control treated group reached EAE score of 2 or higher. Cerebella were homogenized using the method described above and CD11b⁺Tmem119⁺ microglia (~20,000 per sample) were FACS sorted into 500µl RLT buffer (QIAGEN) and stored on -80°C.

STING binding assay

For the nitrocellulose membrane-binding assay, ³⁵S-labeled 2'3'-cGAMP was used as a probe (Li et al., 2014). Negatively charged 2'3'-cGAMP and its analogs do not bind the membrane unless they are bound to proteins. ³⁵S-labeled 2'3'-cGAMP (500 pM) was mixed with 100nM mSTING and bound to the membrane. Different small molecules were then titrated to compete with the probe. The autoradiography signals were analyzed using ImageJ.

RNA sequencing

RNA was extracted from isolated microglia using RNeasy Plus Micro kit (QIAGEN) and the quality assessed by Agilent 2100 Bioanalyzer (Stanford PAN facility). About 1ng RNA was converted to cDNA and amplified for 12 cycles using SMART-seq v4 Ultra Low input RNA kit for sequencing (Takara Bio USA) according to manufacturer's instructions. Amplified cDNA was then purified by immobilization on AMPure XP beads. Purified cDNA was normalized and tagged for 5 mins using Nextera XT DNA library prep kit (Illumina). Unique indexes were then added to each sample, which were then amplified for 12 cycles. cDNA was purified using AMPure XP beads and quality assessed by Advanced Analytical Fragment Analyzer (Stanford PAN facility). Samples were then normalized and pooled together and sequenced on Illumina Novaseq 6000 (Novogene) to obtain 150bp paired-end reads.

The quality of fastq files was assessed using FASTQC (v 0.11.4) (Andrews, 2010). Reads were trimmed to 75bp using fastX toolkit (v 0.0.14) (http://hannonlab.cshl.edu/fastx_toolkit/) to remove poor quality segments toward the end of the reads. Trimmed reads were mapped to mouse mm9 reference genome using STAR (v 2.5.1b) (Dobin et al., 2013). Raw read counts were generated with STAR using the GeneCounts function.

QUANTIFICATION AND STATISTICAL ANALYSIS

The following statistical tests (Prism 7) were used unless otherwise noted. Two groups were compared using unpaired Student's t test. One-way ANOVA followed by Dunnett's multiple comparison test was used for drug treatment experiments with more than one drug, and all treatments were compared to vehicle treated controls. Two-way ANOVA followed by Sidak's multiple comparisons was used for experiments with two genotypes and two treatment conditions. For all figures *p < 0.05, **p < 0.01, *** p < 0.001, ****p < 0.0001.

RNA-seq differential expression

Differential expression in RNA-Seq was analyzed using the R DESeq2 package (Love et al., 2014). Read counts were used as input and normalized using built-in algorithms in DESeq2. Pairwise comparisons among the 4 groups were done on all genes and 16570 genes with calculable fold changes (FC) and false discovery rates (fdr) were used for further analysis. Only the genes differentially expressed in at least one comparison (q < 0.05, n = 59) were included in the Principal Component Analysis (PCA) and in the hierarchical clustering. Normed PCA and hierarchical clustering were performed on rlog-transformed data using the ade4 (Dray and Dufour, 2007) and gplots (Warnes et al., 2016) R packages, respectively. False discovery rate was estimated using Benjamini and Hochberg approach (Benjamini and Hochberg, 1995).

Gene Ontology (GO) analysis

Gene Ontology terms defined the gene product properties and covered three domains: cellular component; molecular function and biological process.

For RNA-seq GO analysis, genes were ranked based on the p value of the differential expression analysis between WT PBS and WT GCV. Enrichment for GOs terms within the top 100 genes was tested with the topGO R package using the 16570 genes kept in the analysis as the background (Alexa and Rahnenfuhrer, 2010).

For microfluidic RT-PCR in primary microglia, the GO analysis was performed to identify GO terms with over-representation of genes when the genes upregulated with GCV (\log_2 fold change > 0.1) were compared to all the genes measured by the Fluidigm platform (83 genes).

DATA AND SOFTWARE AVAILABILITY

[Table S2](#) summarizes differentially expressed genes with p- and q- values from RNA-seq dataset between WT PBS versus WT GCV, WT PBS versus STING^{gt/gt} PBS, and STING^{gt/gt} PBS versus STING^{gt/gt} GCV.

The accession number for the raw and normalized RNA sequence data reported in this paper is NCBI GEO: GSE106692.